Kinetics of inhomogeneous cooling in granular fluids

Subir K. Das and Sanjay Puri
School of Physical Sciences, Jawaharlal Nehru University, New Delhi 110067, India
(Received 6 September 2002; published 14 July 2003)

We study the dynamical behavior of a freely evolving granular gas, where the particles undergo inelastic collisions. The velocity and density fields exhibit complex pattern dynamics, which is reminiscent of phase ordering systems. For example, in the initial time regime, the density field stays (approximately) uniform, and the system is said to be in a *homogeneous cooling state* (HCS). At later times, the density field undergoes nonlinear clustering, and the system continues to lose energy in an *inhomogeneous cooling state* (ICS). We quantitatively characterize the HCS→ICS crossover as a function of system parameters. Furthermore, we study nonlinear growth processes in the ICS by invoking analogies from studies of phase ordering dynamics.

DOI: 10.1103/PhysRevE.68.011302 PACS number(s): 47.50.+d

I. INTRODUCTION

There has been much recent interest in the properties of powders or granular materials [1–3], which consist of assemblies of mesoscopic particles with sizes ranging from 10 μm to 1 cm. These materials are of obvious scientific and technological relevance, and exhibit features intermediate to those of solids and fluids. There have been many studies [1–3] of the static properties of these systems, e.g., formation and structure of granular heaps; stress-distribution profiles in sand-piles, etc. The dynamical properties of granular systems are also of great interest. An important characteristic of grains is that they undergo inelastic collisions which dissipate the system energy. Thus, granular systems exhibit interesting dynamical behavior only when the collisional energy loss is compensated by the input of energy from external driving, and the system settles into a (nonequilibrium) steady-state behavior. In this context, experimentalists have considered various standard geometries for agitating granular systems; e.g., horizontal and vertical vibrations on a platform [4], pouring through a chute [5], rotation in a drum [6,7], etc. All of these experimental situations give rise to diverse examples of pattern formation, which have been of great research interest.

In this paper, we focus on the dynamical evolution of an initially homogeneous system of inelastic granular particles. The system is not externally driven in any manner. Therefore, inelastic collisions between particles result in a loss of energy or ''cooling'' of the system. This problem has received considerable attention in the literature [8–22]. In the initial stages, the system is in a *homogeneous cooling state* (HCS), with the density field being approximately uniform [8]. However, the HCS is linearly unstable to fluctuations, and the system evolves into an *inhomogeneous cooling state* (ICS), where particle-rich clusters are formed and grow [9]. This instability occurs only for wavelengths larger than a critical wavelength that depends on the inelasticity parameter [15]. The primary focus of many earlier studies has been the time-dependent evolution of averaged system quantities, e.g., average energy per particle or ''temperature.'' However, this is inadequate because both the HCS and ICS are characterized by strong correlations in the density and velocity fields. In a recent work, van Noije and co-workers [16] and Baldassari *et al.* [22] have undertaken preliminary studies of correlations in the density and velocity fields in the HCS and ICS. In particular, these authors have emphasized the analogy between the ICS and the behavior of a phase-ordering system, i.e., the dynamical evolution of a homogeneous multicomponent mixture that has been rendered thermodynamically unstable by a rapid quench below the critical temperature [23–25].

In this paper, we present detailed results from molecular dynamics (MD) simulations of the HCS and ICS. In particular, we focus upon the morphological features of the density and velocity fields in the HCS and ICS, and their nonlinear evolution [26]. We invoke analogies with phase-ordering systems to clarify the evolution of the granular gas; e.g., the dynamical scaling of correlation functions and structure factors, general features of scaling functions, the domain growth laws, etc. Of course, the physical mechanisms driving clustering in both cases are completely different, as we will elucidate later.

This paper is organized as follows. In Sec. II, we provide an overview of analytical and numerical results available for this problem. In Sec. III, we present detailed numerical results from our simulations. Finally, Sec. IV concludes this paper with a summary and discussion of our results.

II. OVERVIEW OF EARLIER RESULTS

A. Analytical results

The HCS was first studied by Haff [8], and corresponds to a state with uniform density and temperature; and a coarse-grained velocity field which is identically zero. The granular temperature is defined as $T=\langle v^2\rangle/d$; where $\langle v^2\rangle$ is the squared average of the granular velocity distribution, d is the dimensionality, and we set the mass of granular particles to unity. The homogeneous system cools in time t as $\dot{T}(t) = -\epsilon\omega(T)T/d$, where $\epsilon=1-e^2$, e being the coefficient of restitution. Here, $\omega(T)$ is the collision frequency at temperature T, and has the approximate form $\omega(T)=\pi^{-1/2}\Omega_d\chi(n)n\sigma^{d-1}T^{1/2}$ [27,16], where $\Omega_d = 2\pi^{d/2}/\Gamma(d/2)$ is the total solid angle and $\chi(n)$ is the pair correlation function at contact for hard spheres with number density n and diameter σ. The initial temperature of the granular fluid is T_0, and we set $\omega(T)=\omega(T_0)(T/T_0)^{1/2}$.

These considerations yield Haff's cooling law for the HCS, $T(t)=T_0(1+[\epsilon\omega(T_0)/2d]t)^{-2}$. It is also useful to consider $\tau(t)$, which is the average number of collisions suffered by a particle till time t. We have

$$\tau(t)=\int_0^t dt'\,\omega(t')=\frac{2d}{\epsilon}\ln\left[1+\frac{\epsilon\omega(T_0)}{2d}t\right]. \qquad (1)$$

In terms of τ, the Haff's cooling law has the simple form $T(\tau)=T_0e^{-(\epsilon/d)\tau}$.

The granular system does not remain in the HCS for all time, as both the velocity and density fields are unstable to fluctuations. The first study of this is due to Goldhirsch and co-workers [9], who proposed a nonlinear *shear instability* mechanism for the growth of inhomogeneities in the density field. A subsequent study of this is due to McNamara [11], who investigated linearized hydrodynamic equations for undriven granular gases [14,15]. A recent, thorough exposition of linear instabilities of the HCS is due to van Noije and co-workers (NE) [16]. These authors demonstrate that a *noise reduction* mechanism leads to transverse instabilities in the velocity field, i.e., short-wavelength fluctuations are eliminated more rapidly due to momentum conservation, resulting in a multivortex pattern on diverging length scales. Pattern formation in the velocity field precedes the emergence of inhomogeneities in the density field, which we discuss next. The growth of the vortex scale is diffusive, i.e., $L_v(\tau)\simeq 2\pi\xi_\perp\sqrt{(\epsilon/d)\tau}$, where $\xi_\perp\simeq\sqrt{(2d/\epsilon)}l_0$, with l_0 being the time-independent mean free path $[l_0=\sqrt{2T}/\omega(T)]$.

The length scale for longitudinal fluctuations behaves as $L_{||}\simeq 2\pi\xi_{||}\sqrt{(\epsilon/d)\tau}$, where $\xi_{||}\simeq(2d/\epsilon)l_0$. However, both the transverse and longitudinal fluctuations are exponentially damped in time. This should be contrasted with the fluctuations in the density field, which are driven by longitudinal velocity fluctuations. These actually grow with time (for length scales $\lambda>\xi_{||}$), and must be saturated by an appropriate nonlinearity. However, the linear stability analysis yields the initial growth dynamics for clusters, i.e., $L(\tau)\simeq L_{||}(\tau)$.

B. Numerical results

The Haff's law for the HCS was confirmed in $d=1$ MD simulations by McNamara and Young [12], and Sela and Goldhirsch [10]; and in $d=2$ MD simulations by Goldhirsch and co-workers [9], McNamara and Young [13], Luding *et al.* [18], and Luding and Herrmann [20]. In particular, Luding *et al.* [18] considered collisions of rough granular particles in $d=2,3$, and confirmed that Haff's law applies for both translational and rotational energies.

As stated earlier, our primary interest is to study the nonlinear regime of pattern dynamics in the ICS. The appearance of the clustering instability was first demonstrated numerically by Goldhirsch and co-workers [9,10], and McNamara and Young [12]. A recent study of this problem is due to Luding and Herrmann (LH) [20], who performed $d=2$ MD simulations for a range of e values and studied the time dependence of the average cluster size $L(t)$. LH argue that their numerical data are consistent with a power-law growth $L(t)\sim t^\theta$, where $\theta\simeq 0.3$. In this context, we should remark that long-time simulations encounter problems with inelastic collapse, where a group of particles may undergo an infinite number of collisions in a finite time period. This problem has been studied in some detail by Bernu and Mazighi [28], and McNamara and Young [12,13]. In their simulations, LH use the so-called *time-of-contact* model [19] to avoid unphysical problems due to inelastic collapse.

Finally, we would like to discuss a recent investigation by Baldassarri *et al.* (BMP) [22], who formulated a simple lattice model to mimic inelastic collisions of granular particles. BMP have obtained an interesting range of analytical and numerical results (in $d=2$) from their model. In particular, they focus upon various aspects of the evolving velocity field, e.g., distribution functions, correlation functions, structure factors, autocorrelation functions, etc. They find that the characteristic scale of the transverse and longitudinal velocity structure factors grows as $L_v\sim\tau^{1/2}$, consistent with the analytical results of NE.

This concludes our overview of earlier work on the kinetics of cooling in inelastic granular fluids. To summarize, there is a good understanding of the HCS, and the HCS $\rightarrow$ICS crossover. However, our understanding of the kinetics of cooling and pattern evolution in the ICS is relatively limited. In the present work, we perform comprehensive simulations of $d=2$ granular fluids for a range of densities and inelasticities. Our goal is to obtain a thorough characterization of nonlinear domain growth in the ICS. In particular, we will highlight the analogies between domain growth in the ICS and phase-ordering dynamics in thermodynamically unstable systems.

III. DETAILED NUMERICAL RESULTS

A. Details of simulations

We use an event-driven algorithm for solving the Newtonian dynamical equations for an assembly of inelastic particles [29]. The collision process conserves momentum, though the energy is continuously dissipated due to the inelastic nature of granular particles. We consider identical hard spheres (monodispersed system) with unit mass ($m=1$) and diameter $\sigma=1$. After a collision between the ith and jth particles, having velocities $\vec{v}_i$ and $\vec{v}_j$, respectively, the new velocities are obtained as $\vec{v}'_{i,j}=\vec{v}_{i,j}-[(1+e)/2][\hat{n}\cdot(\vec{v}_{i,j}-\vec{v}_{j,i})]\hat{n}$ [29]. Here, $\hat{n}$ is the unit vector parallel to the relative position of the particles, pointing from j to i at the time of collision. For elastic collisions, we have $e=1$. For granular materials, $e<1$ in general.

In our simulations, there are two different definitions of time. First, we have *real* time t, which is measured in arbitrary units. Second, we also measure time in units of the number of collisions per particle, which we denote as τ. In the HCS, t and τ are related by Eq. (1). Most of our subsequent results are presented in terms of τ, as this constitutes a more natural measure of time for the present problem.

The initial condition for a run consisted of a homogeneous distribution of circular particles in a $d=2$ box of size $(N_b\sigma)^2$ with periodic boundary conditions. Thus, the average packing fraction is $\phi=\pi N/(4N_b^2)$, where N is the number of particles. We always fix $N_b=256$ and vary N, as specified below. We will usually label our numerical results using the number fraction $n=N/N_b^2$. (For particles of unit diameter, the number fraction and number density are identical.) We initialize the particle velocities with uniformly distributed *amplitudes* in $[0,N_b\sigma]$ and *phases* in $[0,2\pi]$. Thus, the initial value of the average kinetic energy is $E(0)=\langle\vec{v}^2\rangle/2=(N_b\sigma)^2/6$. The particles are allowed to collide elastically for a sufficiently long time, e.g., $\tau=100$, till the velocity profile equilibrates to the Maxwell distribution (which is confirmed numerically). This constitutes the initial condition for our MD simulation of freely evolving inelastic hard spheres.

We characterize the dynamical evolution of the granular gas using various statistical quantities, which are calculated as an average over five independent runs up to $\tau=500$. These are (a) equal-time correlation functions and structure factors for the density and velocity fields, and (b) domain growth laws for the characteristic length scales of the density and velocity fields. The precise definitions of these quantities will be provided subsequently.

Before we conclude this section, it is appropriate to discuss the parameter ranges in our simulations. As stated earlier, we fix the box size as $N_b=256$. Numerical data are obtained for the following parameter sets: (i) $N=30\,000$ (or $n\simeq0.46$, $\phi\simeq0.36$), and e ranging from 0.8 to 0.975 in steps of 0.025. (ii) $e=0.90$, and N ranging from 10 000 to 40 000 in steps of 5000, i.e., $n\simeq0.15$–0.61.

B. Evolution morphologies

Figure 1 shows the evolution of the $d=2$ inelastic granular gas from a homogeneous initial condition. The system parameters were $n\simeq0.46$ and $e=0.90$. The snapshots are labeled by the collision time τ, which refers to the number of collisions per particle. We will always measure time in units of τ, which accounts for the reduced collision frequency due to the cooling process. In Fig. 1, the frames on the left-hand side (LHS) and right-hand side (RHS) refer to the granular velocity field $\vec{v}(\vec{r},\tau)$ and the density field $\psi(\vec{r},\tau)$, respectively. The coarse-grained fields at a lattice point are obtained by averaging over boxes of size $(5\sigma)^2$ centered at that point. To clarify the nature of pattern formation, we have ''hardened'' the velocity field in Fig. 1, i.e., the length of all vectors has been set to unity. The velocity field is assigned the value zero at points with no particles in the associated coarse-graining box. Such points are unmarked in Fig. 1. The density field on the RHS of Fig. 1 is depicted in a binary representation. We introduce the order parameter $\psi(\vec{r},\tau)$ with values $+1(-1)$ at points, where the number density is larger than (less than) the average number density ($n\simeq0.46$, in this case). Regions where $\psi=+1$ are marked gray, and regions where $\psi=-1$ are unmarked.

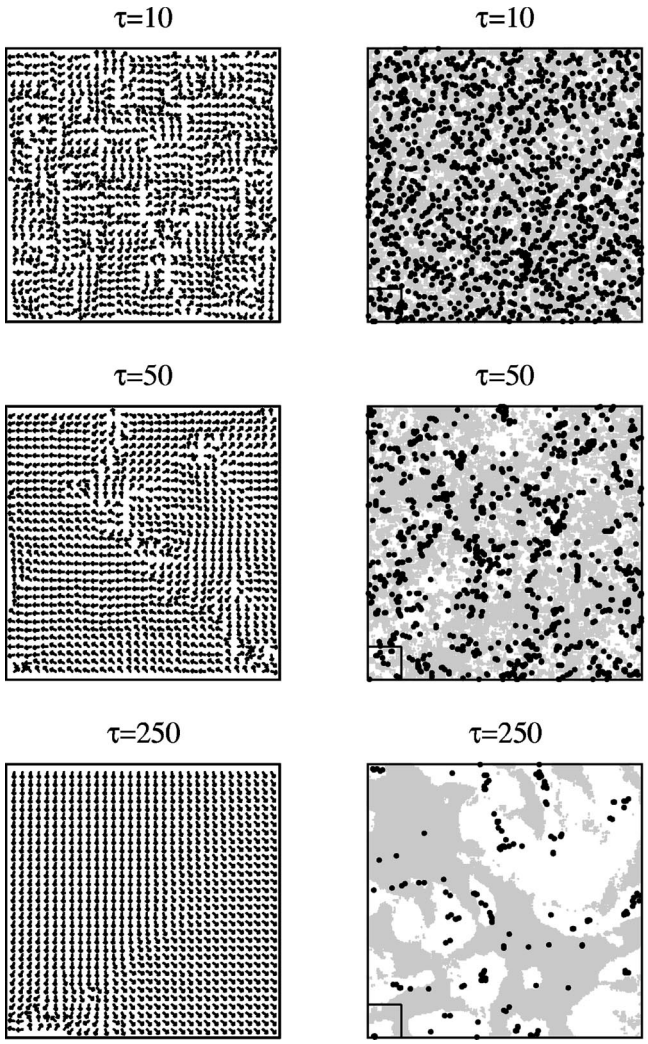

FIG. 1. Evolution of an inelastic granular gas from a homogeneous initial condition. The system density was $n\simeq0.46$; and the restitution coefficient was $e=0.90$. The initial kinetic energy per particle was $E(0)=(N_b\sigma)^2/6$, where $N_b=256$ is the system size and σ is the particle diameter. Further details of the simulation are provided in the text. The frames on the LHS refer to the coarse-grained velocity field. The vector directions correspond to the direction of the local velocity field—the magnitudes have been ''hardened'' to unity. For clarity, we only show a 32^2 corner of the 256^2 lattice, as indicated in the snapshots on the RHS. The frames on the RHS correspond to the coarse-grained density field. Regions where the local density is larger than and less than the average density are marked in grey and white, respectively. The black circles in the RHS frames denote the vortex centers in the velocity field. The snapshots are labeled by the appropriate collision time τ, viz., the average number of collisions per particle.

In Fig. 1, the evolution of the velocity field is characterized by the emergence and diffusive coarsening of vortices. There is a progressive parallelization of the local velocity field due to inelastic dissipation of the normal velocity components. As discussed earlier, pattern evolution in the density field is slower than that for the velocity field. Nevertheless, well-defined clusters corresponding to the ICS are already seen in the snapshot at $\tau=50$. These clusters grow with time

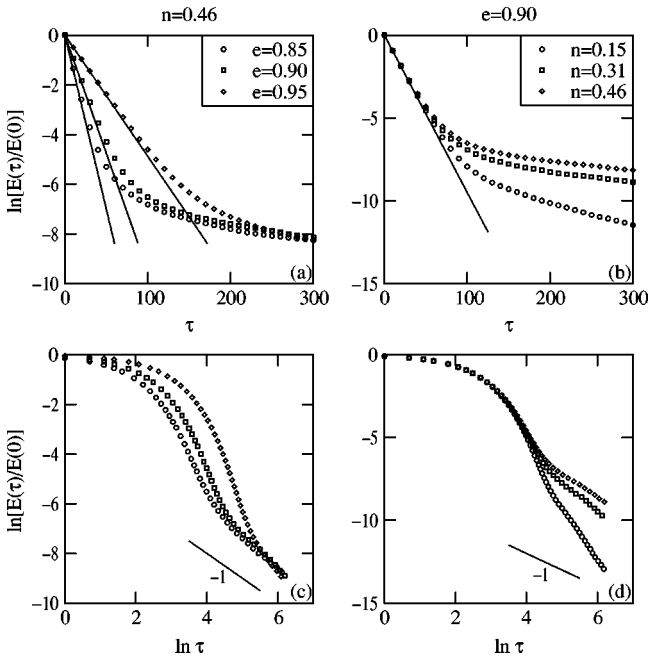

FIG. 2. (a) Plot of $\ln[E(\tau)/E(0)]$ vs τ, where $E(\tau)$ is the average particle energy at time τ. We present data for $n \simeq 0.46$, and $e = 0.85$, 0.90, 0.95, as indicated. The solid lines have slope $-\epsilon/2$ ($\epsilon = 1-e^2$) and correspond to Haff's cooling law in $d=2$. (b) Analogous to (a), but for $e=0.90$ and $n \simeq 0.15$, 0.31, 0.46. The line has slope $-\epsilon/2$. (c) Plot of $\ln[E(\tau)/E(0)]$ vs $\ln \tau$ for the parameter values shown in (a). The solid line has a slope of -1. (d) Analogous to (c), but for the parameter values shown in (b).

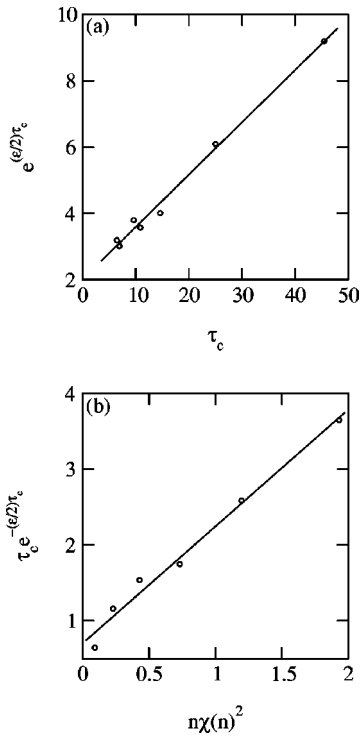

FIG. 3. Dependence of crossover time τ_c for the HCS→ICS transition on system parameters. The crossover time is obtained from the energy plots in Figs. 2(a) and 2(b) as the point of deviation from Haff's law. (a) Plot of $e^{(\epsilon/2)\tau_c}$ vs τ_c for $n \simeq 0.46$; and e ranging from 0.80 to 0.975. The solid line denotes the best linear fit to the data. (b) Plot of $\tau_c e^{-(\epsilon/2)\tau_c}$ vs $n\chi(n)^2$ for $e=0.90$; and n ranging from 0.08 to 0.61. Again, the solid line denotes the best linear fit to the data.

in a manner reminiscent of phase ordering in two-component systems [23]. The vortex centers in the velocity field are also shown (as black circles) in the frames on the RHS. One sees that the vortex density diminishes with time, and the distribution of vortices is primarily confined to regions of low density, as there is a rapid parallelization of velocities in the high-density region due to multiple collision processes. There is no strong correlation between the location of defects in the velocity field (i.e., vortices) and defects in the density field (i.e., interfaces or domain boundaries). Furthermore, the various time scales in this problem, including the emergence of the ICS, diverge as $\epsilon \to 0$ or $e \to 1$.

C. Homogeneous cooling state and crossovers

Let us first briefly focus on the HCS and the HCS→ICS crossover. Figures 2(a) and 2(b) plot $\ln[E(\tau)/E(0)]$ vs τ for a range of (e,n) values. Figure 2(a) corresponds to $n \simeq 0.46$ and $e = 0.85, 0.90, 0.95$. The initial exponential decay corresponds to Haff's cooling law, and the solid lines have slopes $-\epsilon/d$. There is a crossover time τ_c, after which Haff's law does not apply and the cooling rate becomes slower. Similarly, Fig. 2(b) corresponds to $e=0.90$ and $n \simeq 0.15, 0.31, 0.46$. The initial slope is seen to be independent of n (as expected), but the crossover time τ_c does depend on n. In Figs. 2(a) and 2(b), the crossover time is defined as the point of deviation from Haff's law, i.e., where the data points no longer lie on the corresponding solid line.

The crossover time can be estimated from the work of Brito and Ernst [17] as follows. In the HCS, the Haff cooling law is $T(\tau) = T_0 e^{-(\epsilon/d)\tau}$. Brito and Ernst use mode-coupling techniques to obtain the asymptotic energy decay (in the ICS) as

$$T(\tau) \simeq \frac{T_0}{2n}\left(\frac{d-1}{\xi_\perp^d} + \frac{1}{\xi_{||}^d}\right)\left(\frac{4\pi\epsilon}{d}\tau\right)^{-d/2}. \qquad (2)$$

Figures 2(c) and 2(d) test the validity of this asymptotic expression by plotting $\ln[E(\tau)/E(0)]$ vs $\ln \tau$ for the parameter values in Figs. 2(a) and 2(b), respectively. In each case (apart from $n \simeq 0.15, e=0.90$), we see that the asymptotic cooling behavior is consistent with $E(\tau) \sim \tau^{-1}$, i.e., the $d=2$ version of Eq. (2). For the low-density case with $n \simeq 0.15$, it is possible that our simulation has not accessed the asymptotic regime.

A comparison of Haff's law and Eq. (2) yields the crossover time τ_c as the solution of

$$\tau_c^{d/2} e^{-(\epsilon/d)\tau_c} \simeq \frac{(d-1)}{2}\left(\frac{\Omega_d}{4\pi}\right)^d \chi(n)^d n^{d-1}, \qquad (3)$$

where $\sigma = 1$, and we consider the case $\epsilon \to 0$ so that $\xi_{||}[\simeq (2d/\epsilon) l_0] \gg \xi_\perp[\simeq \sqrt{(2d/\epsilon)} l_0]$. For $d=2$, Eq. (3) sim-

plifies as $\tau_c e^{-(\epsilon/2)\tau_c} \sim n\chi(n)^2$, where we ignore the prefactors. Following NE [16], we use the Henderson-Verlet-Levesque approximation [30] for the $d=2$ hard-sphere correlation function at contact, viz.,

$$\chi(n) = \frac{1-7\phi/16}{(1-\phi)^2}, \tag{4}$$

where ϕ is the packing fraction.

Figure 3(a) plots $e^{(\epsilon/2)\tau_c}$ vs τ_c for $n \simeq 0.46$ and a range of e values (specified in the figure caption). Figure 3(b) plots $\tau_c e^{-(\epsilon/2)\tau_c}$ vs $n\chi(n)^2$ for $e=0.90$ and a range of n values (also specified in the figure caption). These approximately linear plots confirm the validity of the scaling behavior of $\tau_c(e,n)$, expected from Eq. (3).

D. Pattern dynamics in the inhomogeneous cooling state

Next, let us focus on the main theme of this paper, viz., quantitative characterization of the pattern morphology, and evolution for the density and velocity fields. In this context, we would like to invoke an analogy between the pattern dynamics in Fig. 1 and the dynamics of phase ordering [24,25]. Of course, the underlying mechanisms of domain growth are quite different in both cases. For example, segregation dynamics in a binary mixture is driven by surface tension (absent in granular materials) between dissimilar components. On the other hand, in the case of granular gases, segregation arises in a purely dynamical context due to the reinforcement of density fluctuations arising from higher collision frequency and faster cooling in regions of high density.

The granular fluid can be described by nonlinear hydrodynamic equations for the density, velocity, and temperature fields, in conjunction with an energy loss term [9]. Wakou *et al.* [31] have shown that fluctuations in these quantities obey time-dependent Ginzburg-Landau (TDGL) equations of phase ordering dynamics with a nonconserved order parameter [24]. In this paper, we elucidate the TDGL description of granular dynamics.

There are two important classes of phase-ordering systems [24,25]: (a) systems with nonconserved order parameter, e.g., ordering of a ferromagnet; (b) systems with conserved order parameter, e.g., phase separation of a binary mixture. The following nonlinear equation describes the nonequilibrium evolution of AB mixtures (in dimensionless units):

$$\frac{\partial \psi(\vec{r},t)}{\partial t} = (-\nabla^2)^m [\psi(\vec{r},t) - \psi(\vec{r},t)^3 + \nabla^2 \psi(\vec{r},t)], \tag{5}$$

where $\psi(\vec{r},t)$ is an order parameter that differentiates between A-rich ($\psi=+1$, say) and B-rich ($\psi=-1$, say) regions. Equation (5) with $m=0$ is referred to as TDGL equation, and describes the systems in class (a) above. The corresponding evolution from a random initial condition is shown in the upper RHS frame of Fig. 4. The coarsening system is characterized by a diffusive growth law $L(t) \sim t^{1/2}$ [23–25]. On the other hand, Eq. (5) with $m=1$ is referred to as the Cahn-Hilliard (CH) equation, and describes the systems in class (b) above. A typical evolution snapshot for the CH equation (from a random initial condition with $\langle \psi \rangle = \psi_0 = -0.08$, as in Fig. 1) is shown in the lower RHS frame of Fig. 4. In this case, the domain growth process is slower and the length scale of the coarsening domains obeys the Lifshitz-Slyozov (LS) law $L(t) \sim t^{1/3}$ [23–25].

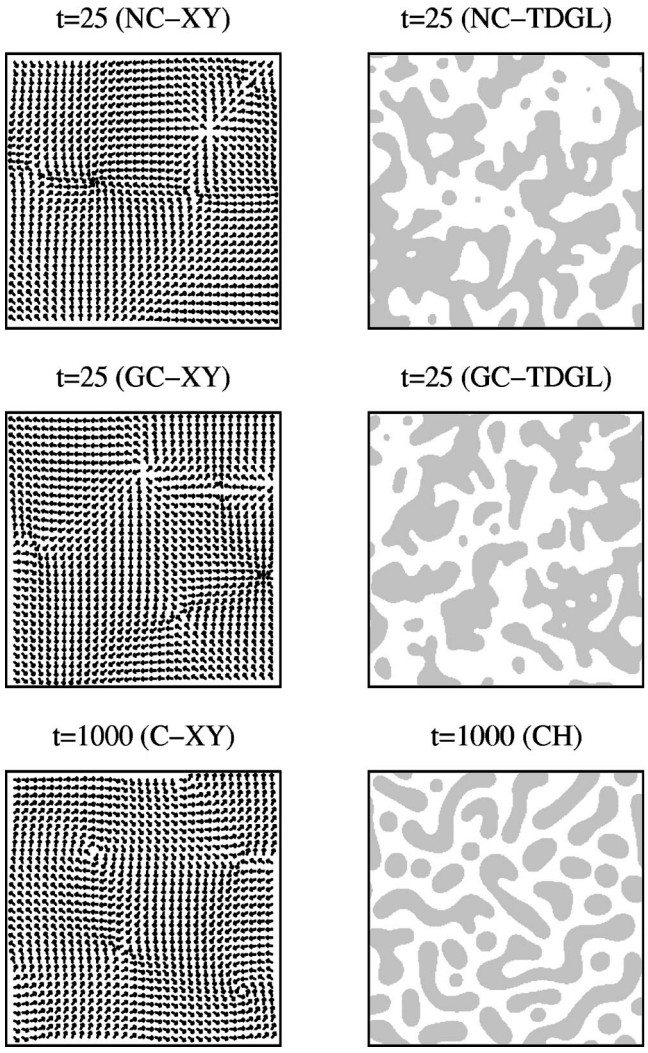

FIG. 4. Evolution pictures from a random initial condition for phase-ordering systems. The lattice size is 256^2, and periodic boundary conditions are applied in both directions. The upper, middle, and lower LHS frames are obtained from simulations of the nonconserved XY (NC-XY) model; globally conserved XY (GC-XY) model with $\langle \vec{\psi} \rangle = 0$; and conserved XY (C-$XY$) model, respectively. The $\vec{\psi}$ field is hardened (i.e., $|\vec{\psi}|=1$) and the direction vectors are plotted in the snapshots on the LHS. For clarity, we only show a 32^2 corner of the 256^2 lattice. The upper, middle, and lower RHS frames are obtained from simulations of the nonconserved TDGL (NC-TDGL) model; globally conserved TDGL (GC-TDGL) model; and CH model, respectively. In the GC-TDGL and CH simulations, the average value of the order parameter is $\langle \psi \rangle = -0.08$, corresponding to an average density of $n=0.46$, as in Fig. 1. Regions with density greater than the average density are marked in grey.

The clustering states in the ICS (Fig. 1) are pictorially similar to the ordering patterns in the TDGL model. This is at

variance with the intuitive expectation that the ICS patterns should be analogous to those in the CH model, because of the conservation law governing the density field. However, the conservation law in the ICS evolution is global rather than local, because particles stream freely across empty spaces and are deposited on distant clusters. In the context of phase ordering dynamics, it is known that systems with global conservation of the order parameter are in the same universality class as systems with nonconserved order parameter [32,33]. The middle RHS frame of Fig. 4 shows an evolution snapshot for the TDGL equation with a global conservation law (referred to as the GC-TDGL equation where GC stands for globally conserved), which enforces $\langle \psi \rangle = -0.08$ (as in Fig. 1). Clearly, the morphologies for the NC-TDGL and GC-TDGL equations are comparable. In this case, NC stands for nonconserved. This pictorial analogy between the ICS and patterns in the TDGL equation will be quantified later, when we present results for correlation functions and structure factors.

Next, let us consider the velocity-field dynamics depicted in the frames on the LHS of Fig. 1. This evolution is reminiscent of coarsening in the XY model [25], which is the two-component generalization of Eq. (5):

$$\frac{\partial \vec{\psi}(\vec{r},t)}{\partial t} = (-\nabla^2)^m [\vec{\psi}(\vec{r},t) - |\vec{\psi}(\vec{r},t)|^2 \vec{\psi}(\vec{r},t) + \nabla^2 \vec{\psi}(\vec{r},t)], \tag{6}$$

where $\vec{\psi} \equiv (\psi_1, \psi_2)$. The evolution in Eq. (6) parallelizes $\vec{\psi}$ locally via the annihilation of vortices and antivortices, driven by the surface-tension reduction mechanism. Equation (6) with $m=0$ corresponds to the case with nonconserved order parameter. A typical evolution picture for this case is shown in the upper LHS frame of Fig. 4. The corresponding domain growth laws [34] are $L_v(t) \sim (t/\ln t)^{1/2}$ for $d=2$ and $L_v(t) \sim t^{1/2}$ for $d>2$. On the other hand, Eq. (6) with $m=1$ corresponds to the conserved XY model [35,36], where the dynamics locally conserves both ψ_1 and ψ_2. A typical evolution snapshot for this case is shown in the lower LHS frame of Fig. 4. The associated domain growth laws for the conserved XY model are $L_v(t) \sim t^{1/4}$ in $d=2$, where the relevant defects are vortices; and $L_v(t) \sim (t \ln t)^{1/4}$ in $d=3$, where the relevant defects are vortex strings [36,37].

Intuitively, we might expect that domain growth in the ICS velocity field is comparable to the conserved XY model as the local parallelization of velocities (due to inelastic dissipation of normal components) occurs in conjunction with momentum conservation. However, because of the streaming of particles over long distances prior to collision, a more appropriate model is the XY equation with global conservation (GC-XY). The middle LHS frame in Fig. 4 shows a typical snapshot for the GC-XY model with $\langle \vec{v} \rangle = 0$. We will now proceed to quantify the pictorial analogies discussed above.

The evolving granular gas is characterized by two length scales in the ICS, i.e., the typical cluster size $L(\tau)$ and the characteristic vortex size $L_v(\tau)$. The existence of these length scales suggests that the morphology is statistically self-similar in time, and only changes by a time-dependent scale factor. Thus, we expect the density correlation function to exhibit the dynamical-scaling property [38]:

$$\begin{aligned} C_{\psi\psi}(r,\tau) &\equiv \frac{1}{V} \int d\vec{R} [\langle \psi(\vec{R},\tau) \psi(\vec{R}+\vec{r},\tau) \rangle \\ &\quad - \langle \psi(\vec{R},\tau) \rangle \langle \psi(\vec{R}+\vec{r},\tau) \rangle] \\ &= g\left(\frac{r}{L(\tau)} \right), \end{aligned} \tag{7}$$

where V is the system volume, and the angular brackets refer to an averaging over independent runs. The correlation functions presented here are always normalized so that $C(0,\tau) = 1$. In Eq. (7), $g(x)$ is the scaling function that characterizes the morphology, and is independent of time. The structure factor of the density field is defined as the Fourier transform of the correlation function, and has the following scaling form:

$$S_{\psi\psi}(k,\tau) \equiv \int d\vec{r} e^{i\vec{k}\cdot\vec{r}} C_{\psi\psi}(r,\tau) = L(\tau)^d \tilde{g}(kL(\tau)). \tag{8}$$

For the velocity field, we study the isotropized correlation function

$$\begin{aligned} C_{vv}(r,\tau) &\equiv \frac{1}{V} \int d\vec{R} [\langle \vec{v}(\vec{R},\tau) \cdot \vec{v}(\vec{R}+\vec{r},\tau) \rangle \\ &\quad - \langle \vec{v}(\vec{R},\tau) \rangle \cdot \langle \vec{v}(\vec{R}+\vec{r},\tau) \rangle] \\ &= h\left(\frac{r}{L_v(\tau)} \right), \end{aligned} \tag{9}$$

where $L_v(\tau)$ is the characteristic length scale of the velocity field. Definition in Eq. (9) averages correlation functions for the transverse and longitudinal components of the velocity field, which evolve on different time scales in the linearized regime [16]. The averaging procedure is reasonable when the patterns are isotropic and the $\vec{k}$ vectors are randomly oriented. The structure factor of the velocity field, $S_{vv}(k,\tau)$, is obtained as the Fourier transform of $C_{vv}(r,\tau)$.

The correlation functions and structure factors presented here are always computed for hardened coarse-grained fields. Thus, the fluctuations in the order-parameter field are set to ± 1, as depicted on the RHS of Fig. 1. Similarly, the amplitude of the velocity field is set to unity, $|\vec{v}(\vec{r},\tau)| = 1$, as depicted on the LHS of Fig. 1. This procedure clarifies the tail regime of the relevant structure factor, which corresponds to scattering from the cores of individual defects. There is a slight violation of the conservation laws due to hardening, but we have confirmed numerically that this is negligible. As mentioned earlier, all statistical quantities presented here are obtained as averages over five independent runs.

Figure 5(a) examines the dynamical-scaling property of the density correlation function for $(n,e) = (0.46, 0.90)$. This figure superposes data for $C_{\psi\psi}(r,\tau)$ vs r/L from three different times (with $\tau \gg \tau_c$) for the evolution depicted in Fig. 1. The characteristic length L is defined as the distance

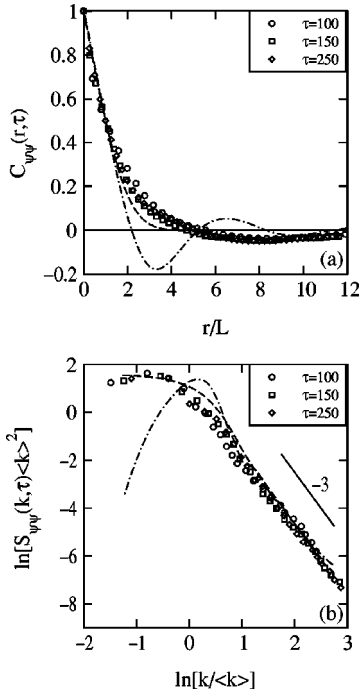

FIG. 5. (a) Dynamical scaling of density correlation function $C_{\psi\psi}(r,\tau)$ for the evolution depicted on the RHS of Fig. 1 (with $n \simeq 0.46$ and $e=0.90$). We superpose data for $C_{\psi\psi}(r,\tau)$ vs r/L from three different times (denoted by the specified symbols) with $\tau \gg \tau_c$. The characteristic length $L(\tau)$ is defined as the distance over which the correlation function decays to half its maximum value. The definition of $C_{\psi\psi}(r,\tau)$, and the relevant averaging statistics, is provided in the text. The dashed line denotes the OJK function in Eq. (10). The dot-dashed line denotes the scaled correlation function (at $t=1000$) for a phase-separating lattice gas with the same average density, i.e., $n \simeq 0.46$. (b) Scaling plots of the structure factors corresponding to (a). We superpose data for $\ln[S_{\psi\psi}(k,\tau)\langle k\rangle^2]$ vs $\ln[k/\langle k\rangle]$ from three different times. The dashed line denotes the OJK function, and the dot-dashed line denotes the scaled structure factor (at $t=1000$) for a phase-separating system with average density $n \simeq 0.46$. The solid line has a slope of -3 and corresponds to the $d=2$ Porod's law, which characterizes scattering off the sharp interfaces.

over which the correlation function decays to half its maximum value [$C_{\psi\psi}(0,\tau)=1$]. The data collapse in Fig. 5(a) is reasonable, confirming that the system evolution is described by a single length scale. The dashed line in Fig. 5(a) denotes the analytic result due to Ohta *et al.* (OJK) [39] for ordering in the NC-TDGL equation:

$$g(x)=\frac{2}{\pi}\sin^{-1}(\gamma), \tag{10}$$

where $\gamma=\exp(-r^2/L^2)$. On the other hand, the dot-dashed line denotes the scaled correlation function obtained from a simulation of the CH equation for phase separation. The average density for the CH simulation is chosen to be the same as that for the granular gas, i.e., $\langle\psi\rangle=-0.08$. We have also studied the correlation function for the GC-TDGL equation with $\langle\psi\rangle=-0.08$. It is numerically indistinguishable from the OJK function, except for a limited region ($x>5$), where it has a very small negative value. This is a consequence of the conservation law, which fixes $\int d\vec{r} C(r,t)=0$. For the sake of clarity, we do not present the correlation function for the GC-TDGL equation in Fig. 5(a).

Our numerical results for the correlation function in the ICS are better approximated by the OJK function than the CH function in the region where $C_{\psi\psi}>0$. This provides a confirmation of the pictorial analogy discussed earlier. Let us next discuss some general considerations that determine specific features of the ICS morphologies. For example, the density correlation functions decay linearly for small $x=r/L$ as follows:

$$g(x)\simeq 1-\alpha x+\beta x^3+\text{higher-order terms}, \tag{11}$$

where α,β are constants [25]. This is a consequence of the presence of sharp domain boundaries between grain-rich and grain-poor regions. The nonanalytic small-x behavior of $g(x)$ results in a power-law decay of the structure factor $S_{\psi\psi}(k,\tau)\sim k^{-(d+1)}$ for large k, which is referred to as the Porod tail [40]. Furthermore, the correlation functions obey the sum rule $\int d\vec{r} C_{\psi\psi}(r,\tau)=S_{\psi\psi}(0,\tau)=0$, which is a direct consequence of the conservation law. In the ICS correlation function, this sum rule is satisfied by $C_{\psi\psi}(r,\tau)$ becoming slightly less than zero over an extended range of x values. (This should be contrasted with the CH correlation function, which exhibits marked oscillations before being damped to zero.)

We have mentioned earlier that the cluster growth process (streaming and aggregation) in the ICS obeys a global (rather than local) conservation law. We speculate that the region where $C_{\psi\psi}(r,\tau)<0$ may constitute a nonscaling part of the correlation function, which is pushed out to $r/L=\infty$ as $\tau\to\infty$. In this case, the scaled correlation function would decay monotonically (as $\tau\to\infty$) as in the case with nonconserved order parameter, e.g., Eq. (10). Our numerical results in Fig. 5(a) do not access this regime as yet.

Figure 5(b) shows the dynamical scaling of the structure factors corresponding to Fig. 5(a). In this case, the appropriate scaling length is defined as $L(\tau)\sim\langle k\rangle^{-1}$, where $\langle k\rangle$ is the first moment of the structure factor. In the scaling regime, we expect all definitions of the characteristic length scale to be equivalent upto prefactors [23]. The tail of the structure factors in Fig. 5(b) exhibits the Porod decay, $S_{\psi\psi}(k,\tau)\sim k^{-(d+1)}$, which characterizes scattering off the sharp interfaces [40]. The dashed line denotes the OJK function, which constitutes an excellent fit to our numerical data. Discrepancy for $r/L\geqslant 2$ in Fig. 5(a) is reflected in the small-k data in Fig. 5(b). The scaled structure factor for the CH equation is denoted by a dot-dashed line. Note that the local conservation law for the CH equation results in a power-law behavior for small-k values, $S_{\psi\psi}(k,t)\sim k^4$ as $k\to 0$ [41]. However, the ICS structure factor appears to decay almost monotonically from $k=0^+$, as is usual for structure factors in ordering problems characterized by a nonconserved order parameter. [Of course, global density conservation dictates that $S_{\psi\psi}(0,\tau)=0$.]

Figure 6 shows the dynamical-scaling property for the correlation function [Fig. 6(a)] and structure factor [Fig.

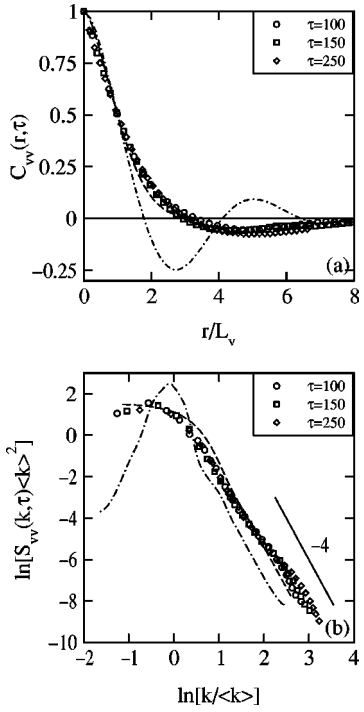

FIG. 6. Analogous to Fig. 5, but corresponding to the coarse-grained velocity field depicted on the LHS of Fig. 1. (a) The dashed line denotes the BPT function in Eq. (12) with $n=2$. The dot-dashed line denotes the scaled correlation function (at $t=1000$) for the conserved XY model [36]. (b) The dashed line denotes the BPT function, and the dot-dashed line denotes the scaled structure factor (at $t=1000$) for the conserved XY model. The solid line has a slope of -4 and corresponds to the $d=2$ generalized Porod's law for scattering off the vortex defects [34].

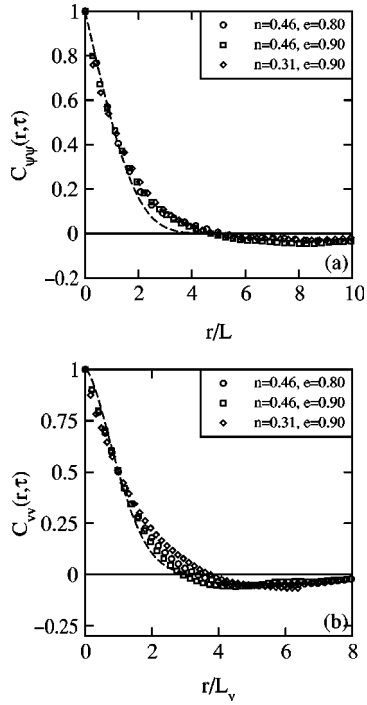

FIG. 7. (a) Comparison of scaled density correlation functions for $(n,e)=(0.46,0.80)$, $(0.46,0.90)$, and $(0.31,0.90)$ (denoted by the specified symbols). Data are computed at collision time $\tau=150$. The dashed line denotes the OJK function. (b) Analogous to (a), but for the velocity correlation functions. Data are computed at collision time $\tau=150$. The dashed line denotes the BPT function.

6(b)] of the velocity field depicted in Fig. 1. In Fig. 6(a), the dashed line denotes the scaled correlation function for the nonconserved XY model in $d=2$. We should point out that the scaled correlation function for the GC-XY model with $\langle\vec{v}\rangle=0$ is numerically indistinguishable from the dashed line in Fig. 6(a). Hence, we do not show the GC-XY result in Fig. 6(a). The analytic result for the NC-XY model [which has O(2) symmetry] was obtained by Puri [34], and generalized to the O(n)-symmetric case by Bray and Puri [34] and Toyoki [34]:

$$h(x)=\frac{n\gamma}{2\pi}\left[B\left(\frac{n+1}{2},\frac{1}{2}\right)\right]^2 F\left(\frac{1}{2},\frac{1}{2};\frac{n+2}{2};\gamma^2\right), \quad (12)$$

where $\gamma=\exp(-r^2/L^2)$; $B(x,y)$ is the β function; and $F(a,b;c;z)$ is the hypergeometric function. Equation (12) is usually referred to as the BPT function. The short-distance behavior of the scaling function is determined by the presence of vortex defects, and has the following form [25,34]:

$$h(x)\simeq 1-\overline{\alpha}x^2\ln x-\overline{\beta}x^2+\text{higher-order terms}, \quad (13)$$

where $x=r/L_v$, and $\overline{\alpha},\overline{\beta}$ are constants. This behavior is common to correlation functions for the inelastic granular gas, as well as for the XY model. The singularity in $h(x)$ as $x\to 0$ yields a power-law decay in the corresponding structure-factor tail, which we will discuss shortly.

In general, the BPT function provides a good approximation to the scaled correlation function for the ICS, except for the region where $C_{vv}(r,\tau)<0$ (resulting from the conservation law). Again, we speculate that the region with $C_{vv}<0$ may comprise a nonscaling portion that is pushed out to $r/L_v=\infty$ as $\tau\to\infty$. For completeness, we also plot in Fig. 6(a) (dot-dashed line) the scaled correlation function for the conserved XY model, which is obtained numerically. Clearly, the velocity-field morphologies in the ICS are comparable to the nonconserved XY model (or GC-XY model) rather than the conserved XY model.

In Fig. 6(b), the structure-factor tails again exhibit a power-law decay but with a different exponent than in Fig. 5(b), i.e., $S_{vv}(k,\tau)\sim k^{-(d+2)}$ for large k. This is also the characteristic of scattering off the defect cores, except the defects in the velocity field are vortices and have an O(2) symmetry. [In general, the BPT function for the case with O(n) symmetry exhibits a "generalized Porod tail," $S(k,t)\sim k^{-(d+n)}$ for a large k.] Furthermore, the BPT function (dashed line) provides a good fit to the numerical data for the ICS velocity field in Fig. 6(b). Again, we see that $S_{vv}(k,\tau)$ decays almost monotonically from $k=0^+$ [though $S_{vv}(0,\tau)=0$], with no marked effects of the conservation law. This should be contrasted with the scaled structure factor for the C-XY model, where C stands for conserved, which is denoted as a dot-dashed line in Fig. 6(b) [36].

Next, let us investigate the functional forms of the scaling

functions across a range of parameter values. Figure 7(a) plots the scaled density correlation functions (all at time $\tau = 150$, $\tau \gg \tau_c$) for $(n,e)=(0.46,0.80)$, $(0.46,0.90)$, and $(0.31,0.90)$. We see that the scaling functions are numerically comparable, indicating that the ICS evolution morphology is equivalent for different parameter values; even though the evolution time scales are quite different. We have confirmed this superuniversal behavior for a wide range of parameter values, and Fig. 7(a) is a representative result. The dashed line in Fig. 7(a) denotes the OJK function. We have confirmed numerically that the scaled correlation function for the GC-TDGL model has a rather weak dependence on the off criticality $\langle \psi \rangle$, and is numerically comparable to the OJK function for a broad range of $\langle \psi \rangle$ values. (Of course, for extreme values of the off-criticality, our numerical data should be compared directly with the data for the GC-TDGL model and not with the OJK function.) This should be contrasted with the case of the CH model, where the correlation function has a sensitive dependence on the off-criticality [23].

Figure 7(b) plots the scaled velocity correlation functions (all at $\tau=150$, $\tau \gg \tau_c$) for the same parameter sets as in Fig. 7(a). The dashed line denotes the BPT function with $n=2$. In this case, the scaled correlation functions differ somewhat for different parameter values. This is a consequence of *holes* in the velocity field, i.e., regions where the coarse-grained velocity field is set to zero because no particles are present in the coarse-graining box. At a fixed time, there are a larger number of holes in the velocity field for the *less elastic* and *less dense* cases, and a correspondingly larger deviation from the BPT function. The appearance of holes in the coarse-grained velocity field can be reduced by choosing larger coarse-graining boxes. However, an upper limit on the box size is set by the core size of vortex defects.

For the time regimes considered here, a description in terms of two uncoupled order parameters is reasonable. A more complete description of the asymptotic ordering dynamics, which accounts for the holes in the velocity field, is provided by a model with spin-vacancy phase separation, in conjunction with XY-like ordering of the spin variable. This is a generalization [42] of the Blume-Emery-Griffiths model [43], where the spin exhibits an up-down ordering behavior. In the current context, the relevant model has coupled nonconserved (or globally conserved) dynamics for the two ordering fields. At a later stage, we will discuss in detail the applicability of this model to the ICS [44].

Apart from the scaled correlation functions and structure factors, it is also relevant to investigate the time dependence of various length scales in the evolving system. We have already discussed how the length scales for density clusters [i.e., domain size $L(\tau)$] and the velocity field [i.e., vortex size $L_v(\tau)$] are obtained from the correlation functions. There is no surface tension between unlike domains in the present case, so domain growth is driven by the diffusive motion of defects. Therefore, we expect that $L(\tau), L_v(\tau) \sim \tau^{1/2}$, in accordance with the arguments of NE [16]. Figure 8(a) plots data for $\ln[L(\tau)]$ vs $\ln \tau$ for the three sets of (n,e) values shown in Fig. 7. There is an initial transient period with no domain growth, corresponding to the HCS (see Fig. 2). Subsequently, well-formed clusters grow in size as seen in Fig. 1. Unfortunately, our numerical data for the length scale is inconclusive regarding the asymptotic dependence of $L(\tau)$ on τ. In part, numerical problems with inelastic collapse limit the time window over which length-scale data are available. Our data are broadly consistent with diffusive growth ($L(\tau) \sim \tau^{1/2}$), but more comprehensive simulations are required for a conclusive result.

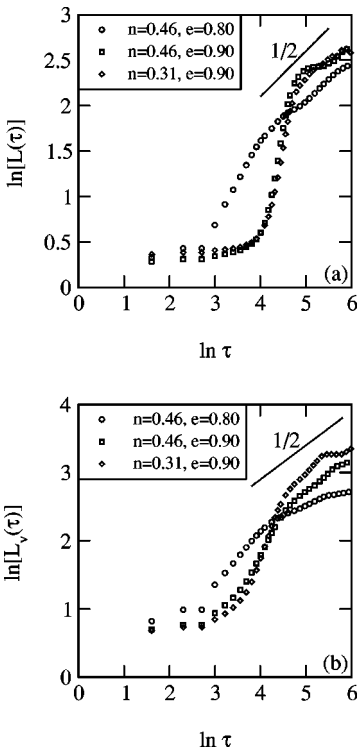

FIG. 8. (a) Plot of $\ln L(\tau)$ vs $\ln \tau$, where the characteristic length scale $L(\tau)$ is obtained from the density correlation function. We present data for $(n,e)=(0.46,0.80),(0.46,0.90),(0.31,0.90)$ (denoted by the specified symbols). The solid line has a slope of 1/2, and corresponds to diffusive growth. (b) Analogous to (a), but for the characteristic length scale of the velocity field, $L_v(\tau)$.

Figure 8(b) plots data for $\ln[L_v(\tau)]$ vs $\ln \tau$ for the same sets of (n,e) values as in Fig. 8(a). Again, our results are inconclusive regarding the asymptotic dependence of $L_v(\tau)$ on τ. For example, the dataset for $(n \simeq 0.46,\ e=0.90)$ is consistent with diffusive growth, $L_v(\tau) \sim \tau^{1/2}$, over an extended time range. However, the same is not true for the other datasets shown.

Finally, Fig. 9 examines the relationship between real time t and the collision time τ. For an elastic granular gas ($e=1$), we expect the relationship to be linear. For the inelastic granular gas ($e<1$), there is a complex relationship between t and τ. In the HCS, $\tau(t)$ is given by Eq. (1). Figure 9(a) plots $e^{\epsilon\tau/4}$ vs t for early times—the resultant linear plot confirms the validity of Eq. (1). As a matter of fact, the scaling relationship in Eq. (1) is valid well beyond t_c (or τ_c). The appropriate values of t_c are specified in the figure caption.

Figure 9(b) plots $\ln(\tau-\tau_c)$ vs. $\ln(t-t_c)$ for the same parameter values as in Fig. 9(a). The numerical data in Fig.

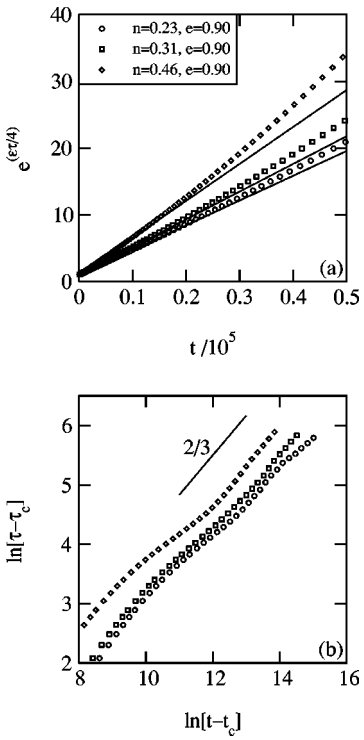

FIG. 9. Dependence of collision time τ on real time t. (a) Plot of $e^{(\epsilon\tau/4)}$ vs $t/10^5$ for early times. We present data for $e=0.90$ and $n \simeq 0.23$, 0.31, 0.46, as indicated. The crossover (real) times for these parameter values are $t_c \simeq 9565$ ($n \simeq 0.23$); $t_c \simeq 7582$ ($n \simeq 0.31$); and $t_c \simeq 1906$ ($n \simeq 0.46$). The solid lines correspond to Eq. (1). (b) Plot of $\ln[\tau-\tau_c]$ vs $\ln[t-t_c]$ for the same parameter values as in (a). The solid line has a slope of 2/3.

9(b) is consistent with the asymptotic power-law behavior, $\tau(t) \sim t^{2/3}$. We see the same scaling behavior for a wide range of parameter values. If we assume a diffusive behavior for the length scales, we see that their asymptotic behavior in real time is $L(t), L_v(t) \sim t^{1/3}$. This result for cluster length scales is consistent with the earlier result of LH [20]. Coincidentally, this domain growth law for the density field in the ICS is the same as the LS growth law for phase separation of binary mixtures. Of course, as we have stressed earlier, the physical reasons for segregation in both cases are quite different.

IV. SUMMARY AND DISCUSSION

Let us conclude this paper with a summary and discussion of the results presented here. We have undertaken a comprehensive MD simulation of a $d=2$ gas of freely evolving inelastic granular particles. The grains are monodispersed, smooth, and hard, and their collisions conserve momentum but dissipate energy. Our simulation uses an event-driven algorithm, and is performed for a wide range of inelasticity and density parameters.

We started off by reviewing the phenomenology, and analytical and numerical results available for this problem. The granular gas initially loses energy in a HCS, where the density field is essentially uniform but the velocity field exhibits vortexlike structures. As particles collide, there is a local parallelization of velocities as normal velocities are dissipated. However, the overall momentum is conserved. Thus, the evolution of the velocity field is reminiscent of ordering dynamics in the XY model. However, the underlying mechanism for domain growth in the velocity field for the granular gas is the diffusive motion of vortex defects, rather than vortex annihilation due to surface tension—as in the XY model.

The fluctuations in the velocity field drive the growth of inhomogeneities in the density field. After a crossover time τ_c, the growing fluctuations in the density field saturate and the system evolves into ICS. For times $\tau \gg \tau_c$, there is a complex pattern formation and evolution in both the density and velocity fields. Earlier works [8–22] have enabled a good understanding of the HCS and the instability which gives rise to the ICS. However, there has been no clear characterization of the asymptotic behavior of nonlinear domain growth processes in the ICS.

In this paper, we have focused on understanding the pattern dynamics in the ICS. We find that the ordering morphology of the density field is comparable to the phase ordering in a ferromagnet (i.e., case with nonconserved order parameter); and the evolution of the velocity field is equivalent to the ordering dynamics of the nonconserved XY model. Of course, there is an overall conservation of density and momentum. However, this is manifested in the form of a global (rather than local) conservation law, because particles stream over extended distances and are deposited on distant clusters. In the context of phase ordering dynamics, it is well known that global conservation laws do not play an important role in determining the evolution dynamics or morphology [32,33].

It is useful to quantify the evolution morphologies in the ICS using correlation functions, structure factors, and domain growth laws. We find that the nature of defects, e.g., domain walls, vortices, determines short-distance singularities in the scaled correlation functions; and large-wave-vector power-law decays of the scaled structure factors. There is a good understanding of these singularities in the context of phase-ordering systems, and the available results are directly applicable in the present context. More generally, the scaled correlation functions and structure factors in the ICS are in good agreement with analytic results for nonconserved ordering fields. There are some differences due to global conservation laws, which require that $\int d\vec{r} C_{\psi\psi}(r,\tau) = S_{\psi\psi}(0,\tau) = 0$, and $\int d\vec{r} C_{vv}(r,\tau) = S_{vv}(0,\tau) = 0$. This is only possible if there are regions in which $C_{\psi\psi}(r,\tau), C_{vv}(r,\tau) < 0$. We speculate that these regions may constitute nonscaling portions of the correlation functions, which vanish as $\tau \to \infty$.

ACKNOWLEDGMENTS

S.P. would like to thank H. Hayakawa for useful discussions and critical inputs on this problem. He is also grateful to M. H. Ernst, I. Goldhirsch, S. Luding, U. M.-B. Marconi, and H. Nakanishi for helpful discussions in this regard. S.K.D. acknowledges financial assistance from the University Grants Commission, India.

[1] H.M. Jaeger, S.R. Nagel, and R.P. Behringer, Rev. Mod. Phys. **68**, 1259 (1996).
[2] *Granular Matter: An Interdisciplinary Approach*, edited by A. Mehta (Springer-Verlag, New York, 1994).
[3] *Powders and Grains 97: Proceedings of the Third International Conference on Powders and Grains*, edited by R.P. Behringer and J. Jenkins (Balkema, Rotterdam, 1997); *Powders and Grains 2001: Proceedings of the Fourth International Conference on Powders and Grains*, edited by T. Kishino (Swets and Zeitlinger, Lisse, 2001).
[4] F. Melo, P.B. Umbanhowar, and H.L. Swinney, Phys. Rev. Lett. **75**, 3838 (1995); P.B. Umbanhowar, F. Melo, and H.L. Swinney, Nature (London) **382**, 793 (1996).
[5] G. Peng and H.J. Herrmann, Phys. Rev. E **49**, R1796 (1994); **51**, 1745 (1995); O. Moriyama, N. Kuroiwa, M. Matsushita, and H. Hayakawa, Phys. Rev. Lett. **80**, 2833 (1998).
[6] J. Rajchenbach, Phys. Rev. Lett. **65**, 2221 (1990); S. Das Gupta, D.V. Khakhar, and S.K. Bhatia, Chem. Eng. Sci. **46**, 1531 (1991); Powder Technol. **67**, 145 (1991); O. Zik, D. Levine, S.G. Lipson, S. Shtrikman, and J. Stavans, Phys. Rev. Lett. **73**, 644 (1994).
[7] For modeling and analytical results on this problem, see S. Puri and H. Hayakawa, Physica A **290**, 218 (2001); **270**, 115 (1999).
[8] P.K. Haff, J. Fluid Mech. **134**, 401 (1983).
[9] I. Goldhirsch and G. Zanetti, Phys. Rev. Lett. **70**, 1619 (1993); I. Goldhirsch, M.-L. Tan, and G. Zanetti, J. Sci. Comput. **8**, 1 (1993).
[10] N. Sela and I. Goldhirsch, Phys. Fluids **7**, 507 (1995).
[11] S. McNamara, Phys. Fluids A **5**, 3056 (1993).
[12] S. McNamara and W.R. Young, Phys. Fluids A **4**, 496 (1992); **5**, 34 (1993).
[13] S. McNamara and W.R. Young, Phys. Rev. E **53**, 5089 (1996).
[14] J.J. Brey, F. Moreno, and J.W. Dufty, Phys. Rev. E **54**, 445 (1996); J.J. Brey, F. Moreno, and M.J. Ruiz-Montero, Phys. Fluids **10**, 2965 (1998); **10**, 2976 (1998).
[15] J.J. Brey, M.J. Ruiz-Montero, and D. Cubero, Phys. Rev. E **54**, 3664 (1996); **60**, 3150 (1999).
[16] T.P.C. van Noije, M.H. Ernst, R. Brito, and J.A.G. Orza, Phys. Rev. Lett. **79**, 411 (1997); T.P.C. van Noije, M.H. Ernst, and R. Brito, Phys. Rev. E **57**, R4891 (1998); T.P.C. van Noije and M.H. Ernst, *ibid.* **61**, 1765 (2000).
[17] R. Brito and M.H. Ernst, Europhys. Lett. **43**, 497 (1998).
[18] S. Luding, M. Huthmann, S. McNamara, and A. Zippelius, Phys. Rev. E **58**, 3416 (1998).
[19] S. Luding and S. McNamara, Granular Matter **1**, 113 (1998).
[20] S. Luding and H.J. Herrmann, Chaos **9**, 673 (1999).
[21] H. Nakanishi and N. Mitarai, in *Powders and Grains 2001: Proceedings of the Fourth International Conference on Powders and Grains*, edited by T. Kishino (Swets and Zeitlinger, Lisse, 2001).
[22] A. Baldassarri, U.M.-B. Marconi, and A. Puglisi, Phys. Rev. E **65**, 051301 (2002); U.M.-B. Marconi (private communication).
[23] Y. Oono and S. Puri, Phys. Rev. Lett. **58**, 836 (1987); Y. Oono and S. Puri, Phys. Rev. A **38**, 434 (1988); S. Puri and Y. Oono, *ibid.* **38**, 1542 (1988).
[24] K. Binder, in *Materials Science and Technology, Phase Transformations of Materials*, edited by R.W. Cahn, P. Haasen, and E.J. Kramer (VCH, Weinheim, 1991), Vol. 5, p. 405.
[25] A.J. Bray, Adv. Phys. **43**, 357 (1994).
[26] S.K. Das and S. Puri, Europhys. Lett. **61**, 749 (2003).
[27] S. Chapman and T.G. Cowling, *The Mathematical Theory of Non-Uniform Gases* (Cambridge University Press, Cambridge, 1970).
[28] P. Bernu and R. Mazighi, J. Phys. A **23**, 5745 (1990).
[29] M.P. Allen and D.J. Tildesley, *Computer Simulation of Liquids* (Oxford University Press, Oxford, 1987).
[30] D. Henderson, Mol. Phys. **30**, 971 (1975); L. Verlet and D. Levesque, *ibid.* **46**, 969 (1982).
[31] J. Wakou, R. Brito, and M.H. Ernst, J. Stat. Phys. **107**, 3 (2002).
[32] F.F. Annett and J.R. Banavar, Phys. Rev. Lett. **68**, 2941 (1992); A.J. Bray, *ibid.* **66**, 2048 (1991).
[33] C. Sire and S.N. Majumdar, Phys. Rev. E **52**, 244 (1995).
[34] A.J. Bray and S. Puri, Phys. Rev. Lett. **67**, 2670 (1991); S. Puri, Phys. Lett. A **164**, 211 (1992); H. Toyoki, Phys. Rev. B **45**, 1965 (1992).
[35] M. Mondello and N. Goldenfeld, Phys. Rev. E **47**, 2384 (1993).
[36] S. Puri, A.J. Bray, and F. Rojas, Phys. Rev. E **52**, 4669 (1995); F. Rojas, S. Puri, and A.J. Bray, J. Phys. A **34**, 3985 (2001).
[37] A.J. Bray and A.D. Rutenberg, Phys. Rev. E **49**, R27 (1994); A.D. Rutenberg and A.J. Bray, *ibid.* **51**, 5499 (1995).
[38] K. Binder and D. Stauffer, Phys. Rev. Lett. **33**, 1006 (1974); Z. Phys. B **24**, 406 (1976).
[39] T. Ohta, D. Jasnow, and K. Kawasaki, Phys. Rev. Lett. **49**, 1223 (1982).
[40] G. Porod, in *Small-Angle X-Ray Scattering*, edited by O. Glatter and O. Kratky (Academic, New York, 1982); Y. Oono and S. Puri, Mod. Phys. Lett. B **2**, 861 (1988).
[41] C. Yeung, Phys. Rev. Lett. **61**, 1135 (1988).
[42] B.P. Lee (unpublished).
[43] M. Blume, V.J. Emery, and R.B. Griffiths, Phys. Rev. A **4**, 1071 (1971).
[44] S. Puri (unpublished).